Chemical Engineering Journal 185–186 (2012) 168–177

Contents lists available at SciVerse ScienceDirect

Chemical Engineering Journal

journal homepage: www.elsevier.com/locate/cej

Investigation of solid catalysts for glycolysis of polyethylene terephthalate

Minli Zhu[a], Shan Li[a], Zengxi Li[a,*], Xingmei Lu[b,**], Suojiang Zhang[b]

[a] College of Chemistry and Chemical Engineering, Graduate University of Chinese Academy of Sciences, Beijing 100049, PR China
[b] Beijing Key Laboratory of Ionic Liquids Clean Process, Institute of Process Engineering, Chinese Academy of Sciences, Beijing 100190, PR China

ARTICLE INFO

Article history:
Received 4 November 2011
Received in revised form 12 January 2012
Accepted 12 January 2012

Keywords:
Polyethylene terephthalate
Glycolysis
Solid acid catalyst
Characterization

ABSTRACT

Three series of solid catalysts including SO_4^{2-}/ZnO, SO_4^{2-}/TiO_2 and $SO_4^{2-}/ZnO\text{-}TiO_2$ were prepared by precipitation or co-precipitation method with different calcination temperature. The textural properties of the catalysts were studied by means of XRD, Raman, SEM, N_2 adsorption–desorption and energy dispersive X-ray analysis. Acidity properties of the catalysts were tested by NH_3–TPD and pyridine–FTIR methods. Glycolysis of Polyethylene terephthalate (PET) into monomer of bis(2-hydroxyethyl terephthalate) (BHET) over solid acid catalysts has been studied. Relationships between the textural properties, the surface acidity and the catalytic activity have been investigated. Experimental results showed that the surface area and the amount of middle strength acid sites on the sulfated binary oxides of $SO_4^{2-}/ZnO\text{-}TiO_2$-200–300 °C were higher than those on unitary oxide of zinc or titanium. The FTIR study showed that the Lewis acid sites predominated over the $SO_4^{2-}/ZnO\text{-}TiO_2$-300 °C catalyst, while the peak corresponding to Brönsted acid sites was weak or absent. The $SO_4^{2-}/ZnO\text{-}TiO_2$-200–300 °C exhibited a catalytic activity with 100% conversion of PET and 72% selectivity of BHET after 3 h at 180 °C under atmospheric pressure. The catalyst has been reused for four times and the catalytic activity of recycled catalyst maintained the same as that of the fresh catalyst.

1. Introduction

Polyethylene terephthalate (PET) is a kind of semi-crystalline, thermoplastic polyester with high strength and transparency properties. Because of these properties, PET is produced in considerable amount and is used in textile industry, high strength fibers and soft drink bottles [1]. With the widespread use and increasing consumption of PET, the amount of discarded PET is growing rapidly, and accompanied environmental problems are becoming more and more serious [2,3]. Therefore recycling the discarded PET polymer is an efficient approach to reduce the consumption of resources and to protect the environment at the same time [4,5]. PET is a kind of polyester with functional ester groups that can be cleaved by reagents, such as water, acids or bases (hydrolysis) [6,7], alcohols (alcoholysis) [8], amines (aminolysis) [9,10], ammonia (ammonolysis) [9] and glycols (glycolysis) [5,11–13]. Particularly, the glycolysis reaction is the molecular degradation of PET polymer by glycols, typically ethylene glycol. The ester linkages of PET polymer are broken and replaced by hydroxyls terminals to give bis(2-hydroxyethyl terephthalate) (BHET), which is the raw material of producing PET [12]. Glycolysis of PET is most frequent process by using metal acetates (Zn, Co, Pb and Mn) as catalysts [3,11,14]. The catalytic activity with these homogeneous catalysts is high. However, they have several drawbacks, such as the catalyst cannot be easily separated from the reaction mixture, the existence of side reactions, and the purity of products [15,16].

In recent decades, solid acids have attracted great attention as environmentally benign catalysts in most chemical processes [17,18]. The solid acids have many advantages over homogeneous acids, such as non-corrosive, easy separation by filtration, and less waste production through recycling [15,19,20]. Among them there are sulfated oxides such as sulfated zirconia, titania and iron oxide, which have exhibited high thermostability, superacid property and high catalytic activity [21–23].

In this paper we report a study of three series of solid acid catalysts (SO_4^{2-}/ZnO, SO_4^{2-}/TiO_2 and $SO_4^{2-}/ZnO\text{-}TiO_2$) on glycolysis of PET, which have not yet been extensively studied. The effect of the calcination temperature on textural properties was obtained by XRD, Raman spectrum and the adsorption of N_2 techniques. The nature of acid sites of catalysts was revealed by the aid of NH_3–TPD and FTIR of adsorbed pyridine. The aim of this paper is to evaluate the relationships between textural, acid properties and catalytic activity.

---

* Corresponding author. Tel.: +86 10 88256322; fax: +86 10 88256322.
** Corresponding author. Tel.: +86 10 82544800; fax: +86 10 82627080.
E-mail addresses: zxli@home.ipe.ac.cn (Z. Li), xmlu@home.ipe.ac.cn (X. Lu).

1385-8947/$ – see front matter © 2012 Elsevier B.V. All rights reserved.
doi:10.1016/j.cej.2012.01.068

2. Experimental

2.1. Catalyst preparation

SO_4^{2-}/ZnO-TiO_2: Zn-Ti hydroxide gel was prepared by co-precipitation method. Aqueous ammonia (28%) was added dropwise with vigorously stirring into a mixture solution of 0.2 mol/L $Zn(Ac)_2$ and 0.2 mol/L $Ti(SO_4)_2$ to obtain hydroxides until pH reached 8 at room temperature. The solution including precipitation was kept in a water bath warmed at 70 °C for 4 h, and then filtered and washed with deionized water, and dried at 110 °C for 12 h. The powder was pulverized to 140–200 mesh, and then impregnated with 0.5 M $(NH_4)_2SO_4$ sulfate solution (15 mL g^{-1}) under continuous stirring at room temperature for 4 h and then filtered and dried at 110 °C for 12 h. The prepared precursor was calcined at 200, 300, 400, 500 and 600 °C for 3 h, respectively. Each catalyst is stored in a sealed glass ampoule for use. Catalysts of SO_4^{2-}/ZnO and SO_4^{2-}/TiO_2 were prepared by the similar process. Catalysts of SO_4^{2-}/ZnO, SO_4^{2-}/TiO_2 and SO_4^{2-}/ZnO-TiO_2 thus prepared are denoted as S/Zn-°C, S/Ti-°C and S/Zn-Ti-°C in the following based on the calcination temperature.

2.2. Catalyst characterization

X-ray diffraction (XRD) patterns of catalysts were recorded by X'Pert PRO MPD diffractometer operated at an accelerating voltage of 40 kV and an emission current of 40 mA with Cu Kα radiation. The angle (2θ) was measured in steps of 0.41778° s^{-1} between 5° and 90°.

Raman spectroscopy was recorded by a LabRam HR 800 spectrometer (Jobin Yvon-Horiba) with 514.53 nm of an Ar–Kr 2018 RM laser (Spectrum Physics) as the excitation source.

Weight loss and temperature associated with phase transformation were determined by thermogravimetry and differential thermal analysis (TG/DTA) on a Seiko TG/DTA SSC 5000 analyzer. The fresh samples of catalysts before calcination were heated from room temperature to 600 °C at rate of 10 °C min^{-1} in nitrogen flow (30 mL min^{-1}).

The BET specific surface area and the pore size were obtained from nitrogen absorption and desorption isotherm method at liquid nitrogen temperature on a Quanta Chrome Instrument NOVA 2000. Prior to analysis, samples calcined above 300 °C were degassed at 300 °C for 6 h and samples calcined below 300 °C were degassed at 150 °C for 10 h, under 10^{-3} Torr.

TPD of ammonia was performed on an Autochem II 2920 apparatus from Micromeritics. In a typical experiment, 20 mg of catalyst was pretreated in a helium flow at 150 °C at a heating rate of 10 °C min^{-1} and the sample was kept at this temperature for 1 h. Subsequently the sample was treated with a 10% NH_3—He flow for 30 min at room temperature, then the sample was purging in a helium flow for 1 h at 100 °C, until the baseline was stable, the desorption profile was measured by the thermal conductivity detector in flowing helium at a heating rate of 10 °C min^{-1} to 600 °C.

The surface acidity of the catalysts was investigated by means of studying pyridine adsorption on a Fourier transform infrared (FTIR) spectroscopy. Pyridine FTIR spectrum was recorded on a Nicolet 6700 spectrometer equipped with a cell in situ. The sample was pressed into a self-supporting plate (10–15 mg, 13 mm diameter), placed in an IR cell and treated at 150 °C under vacuum (0.0013 Pa) for 1 h. After the IR cell was cooled to room temperature, pyridine vapor was introduced into the cell and adsorbed for 10 min and took 30 min for equilibrium. Then it was scanned after being vacuumed for 15 min and recorded at room temperature, 100 °C, 150 °C, and 250 °C under vacuum.

Scanning electron microscopy (SEM) was taken by using a FEI MLA250 with an acceleration voltage of 20 kV at high vacuum operating mode. Catalyst samples were coated with carbon prior to scanning. The element composition of the catalysts was analyzed by energy dispersive X-ray spectroscopy (EDS).

2.3. Measurement of catalytic activity

PET pellets (2.0 mm × 2.5 mm × 2.7 mm) were pure and supplied by Jindong Commercial Co. Ltd. Jiangsu Province, China. Analytical grade of zinc acetate (≥99.0%), ethylene glycol, ammonia (25%), ammonium sulfate (≥99.0%) and chemical grade of titanium (IV) sulfate (≥96.0%) were obtained from Sinopharm Chemical Reagent Beijing Co., Ltd., China. The materials were used without any further treatment.

In a typical experiment, 5 g of PET and 25 mL ethylene glycol were loaded into a three-neck flask equipped with a thermometer, a reflux condenser and a magnetic stirrer. When the reactant system was heated to 180 °C, 0.015 g of catalyst was added into the system and the reaction was carried out for 3 h. After reaction, the reactor was cooled to room temperature and the undepolymerized PET pellets were quickly separated from the liquid phase before the products precipitated. Then amount of distilled water was used to wash the undepolymerized PET pellets, and the water was then mixed with the product fraction. The undepolymerized PET was collected, dried and weighed. Meanwhile, about 200 mL distilled water was added to the product mixture with vigorously agitated, which would dissolve the remaining EG and the BHET monomer. After the mixture was filtered, the undissolved substance was oligomer, which dried and weighed. And the collected filtrate was concentrated and stored in a refrigerator at 5 °C for overnight. White crystalline flakes of BHET monomers were formed in the filtrate, then separated and dried in an oven at 60 °C.

In this study, the catalytic activity of catalysts on glycolysis of PET was measured by testing the conversion of PET (%) and the selectivity of BHET (%), which were calculated in Eqs. (1) and (2). In Eq. (1), $W_{PET,i}$ is initial weight of PET, $W_{PET,u}$ is weight of unreacted PET [24].

$$\text{Conversion of PET}\,(\%) = \frac{(W_{PET,i} - W_{PET,u}) \times 100\%}{W_{PET,i}} \tag{1}$$

$$\text{Yield of BHET}\,(\%) = \frac{(\text{moles of BHET}) \times 100\%}{(\text{moles of depolymerized PET units})} \tag{2}$$

3. Results and discussion

3.1. Catalyst characterization

3.1.1. XRD results

Figs. 1, 2 and 3 present the XRD patterns of S/Zn, S/Ti and S/Zn-Ti at different calcination temperatures, respectively. The ZnO with hexagonal phase (JCPD-ICDD 01-089-0510) was observed in all the catalysts of S/Zn-200–600. It indicates that the S/Zn-200–600 catalysts exhibited high crystallinity of ZnO (Fig. 1). When the calcination temperature is higher than 200 °C, in addition to the lines of ZnO, a few extra lines due to the formation of $Zn_3O(SO_4)_2$ compound with monoclinic phase (JCPD-ICDD 00-016-0821) could be also noted.

In the case of the S/Ti catalysts, it can be observed from Fig. 2 that the structural changes occurred with increasing the calcination temperature. The catalysts were kept in an amorphous state when calcined below 300 °C and the formation of anatase TiO_2 started when calcined higher than 400 °C. When the calcination temperature was up to 600 °C all the diffraction peaks (2θ = 25.3°, 37.9°, 48.0°, 55.0°) could be identified as anatase TiO_2 (JCPDS 01-084-1286).

The XRD patterns of sulfated binary metal oxides S/Zn-Ti are shown in Fig. 3. The catalysts calcined bellow 400 °C were found

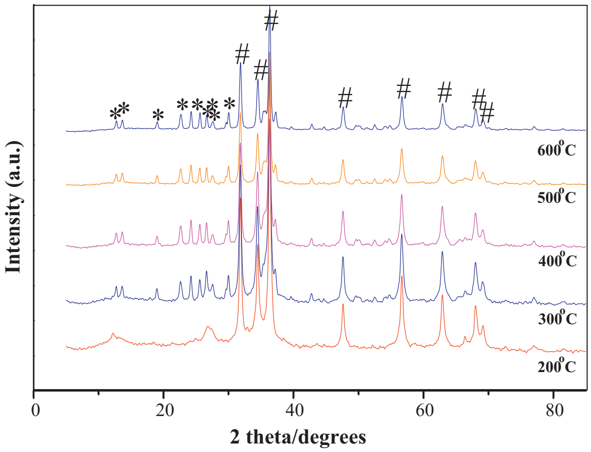

Fig. 1. XRD patterns of S/Zn calcined at different temperatures: (*) $Zn_3O(SO_4)_2$, monoclinic, (#) ZnO, hexagonal.

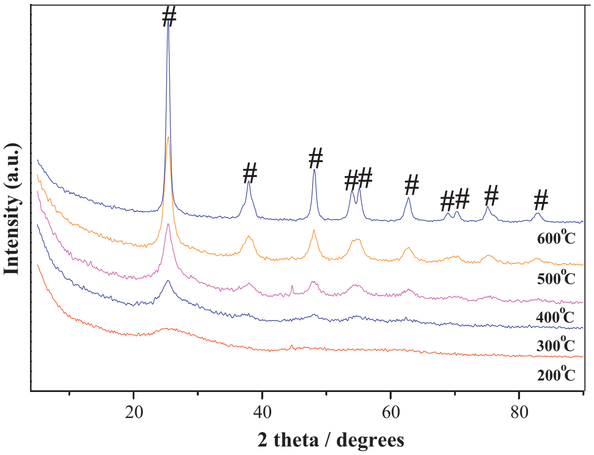

Fig. 2. XRD patterns of S/Ti calcined at different temperatures: (#) TiO_2, anatase.

to be in amorphous state. The formation of TiO_2 (JCPDS 01-084-1286) with anatase phase and $TiZn_2O_4$ (JCPD-ICDD 01-077-0014) with cubic phase started at calcination temperature 500 °C and the diffraction peaks increased with increasing the calcination temperature from 500 to 600 °C. Compared with XRD patterns of S/Zn (Fig. 1), the binary oxides of Zn and Ti inhibited the formation of crystalline in S/Zn-Ti.

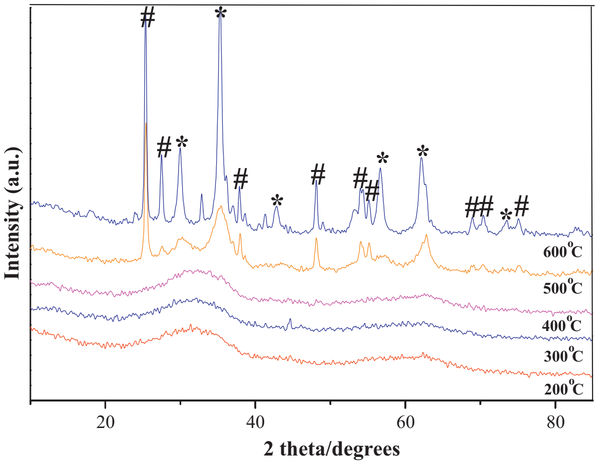

Fig. 3. XRD patterns of S/Zn-Ti calcined at different temperatures: (#) TiO_2, anatase, (*) $TiZn_2O_4$, cubic.

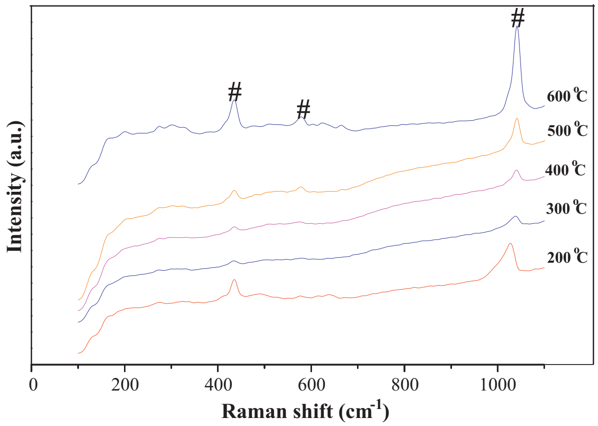

Fig. 4. Raman spectroscopy of S/Zn calcined at different temperatures: (#) ZnO, hexagonal.

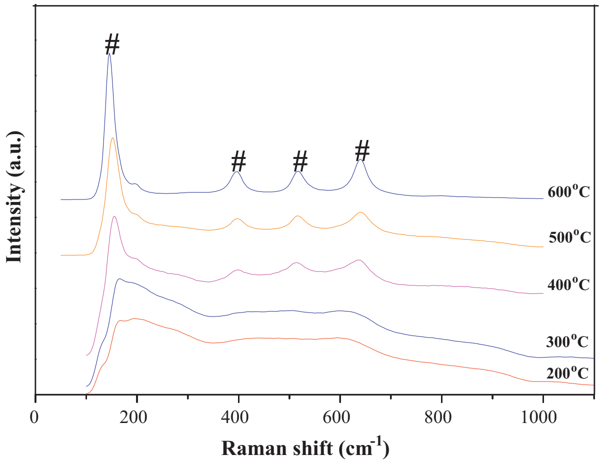

Fig. 5. Raman spectroscopy of S/Ti calcined at different temperatures: (#) TiO_2, anatase.

3.1.2. *Raman spectroscopy*

Raman spectrum can provide complementary structural information of these catalysts. Figs. 4, 5 and 6 show the Raman spectra of three series of S/Zn, S/Ti and S/Zn-Ti catalysts, respectively. For the

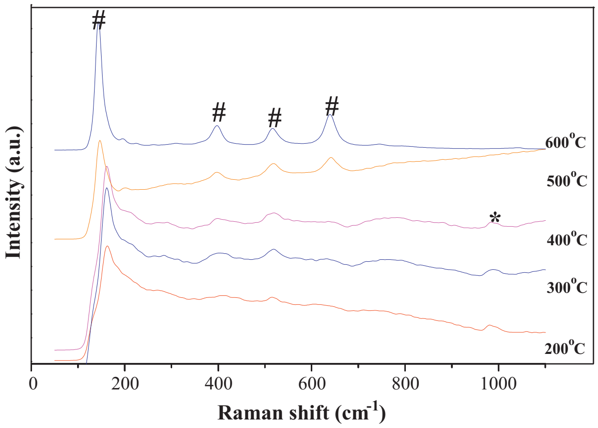

Fig. 6. Raman spectroscopy of S/Zn-Ti calcined at different temperatures: (#) TiO_2, anatase, (*) ZnO, hexagonal.

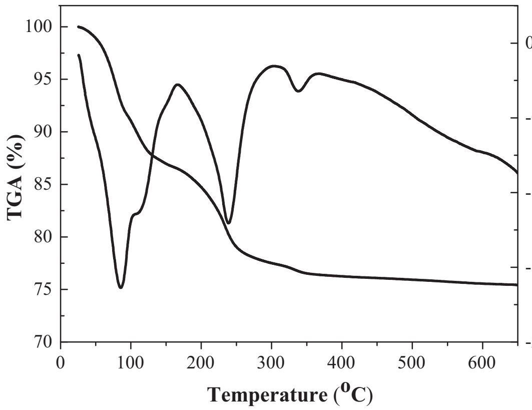

Fig. 7. TG/DTA curves of S/Zn.

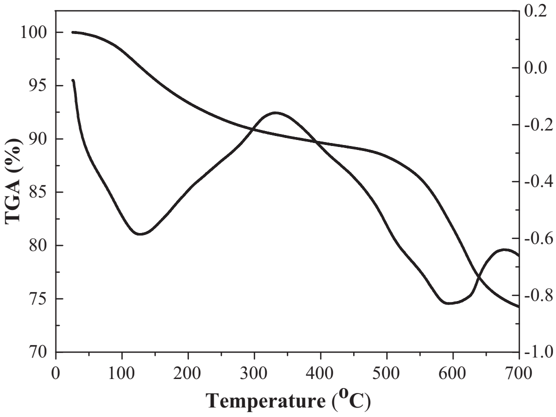

Fig. 8. TG/DTA curves of S/Ti.

Table 1
Sulfur content of the catalysts.

S/Zn-°C	S (wt%)	S/Ti-°C	S (wt%)	S/Zn-Ti-°C	S (wt%)
200	11.5	200	6.5	200	3.6
300	10.2	300	6.1	300	3.3
400	9.9	400	4.5	400	3.1
500	9.8	500	4.3	500	3.1
600	8.5	600	1.6	600	2.9

samples of S/Zn at different calcination temperatures (Fig. 4), the Raman spectra exhibited lines at 435, 577 and 1041 cm^{-1}, which corresponded to ZnO hexagonal structure. Peak located at 435 cm^{-1} is due to E_2 (high frequency) mode. The peak at about 577 cm^{-1} is attributed to the E_1 (LO) mode. The peak at 1041 cm^{-1} is generally assigned to be the second-order vibrational mode [25–27]. The peaks increased with increasing the calcination temperature, which due to the amount of crystalline of ZnO increased. The Raman spectra of S/Ti calcined at 400–600 °C (Fig. 4) exhibited four peaks at 143, 396, 514, and 636 cm^{-1} assigned as Eg, B_{1g}, $A_{1g}+B_{1g}$, and E_g modes, respectively [28,29]. The intensity of peaks increased with increasing the calcination temperature. This indicates the increase of amount of anatase TiO_2 with increasing the calcination temperature, which coincidence with the XRD results. The Raman spectra of S/Zn-Ti at different calcination temperatures are shown in Fig. 5. The Raman spectra of S/Zn-Ti exhibited four peaks at 143, 396, 514, and 636 cm^{-1}, which are associated to TiO_2 anatase structure. A broad peak at 1077 cm^{-1} was discovered on samples of S/Zn-Ti-200–400, which assigned to ZnO species. The peaks were broad and weak on the samples S/Zn-Ti-200–500. This may be due to the high dispersion and/or low crystalline nature (amorphous) of the metal oxides on the S/Zn-Ti-200–500. Furthermore, there were no ZnO related peaks observed on the samples of S/Zn-Ti-500–600, which indicates that the most of the ZnO was actually fixed in the framework of TiO_2 to form the cubic structure of $TiZn_2O_4$. Thus, the Raman results supported the conclusion made by XRD study.

3.1.3. Thermal analysis (TG/DTA)

The thermostability of synthesized catalysts was investigated by TG/DTA method. For the sample of S/Zn (Fig. 7), the first weight loss below 160 °C was 14% accompanied with the first big endothermic DTA peak at 85 °C, which mainly ascribed to the loss of physical adsorbed water molecules. The second weight loss was 10.7% between 160 and 400 °C accompanied with the second big endothermic DTA peak at 238 °C and a relatively small peak at 338 °C, which were attributed to decomposition of interlayer acetate and ammonium and dehydroxylation of the hydrate layers [30]. The weight loss between 400 and 600 °C was 0.7% and no visible endothermic DTA peak was observed. This indicates no further decomposition of compounds in the catalyst. For the sample of S/Ti (Fig. 8), the weight loss between 100 and 400 °C was 10.4% and had a broad endothermic DTA peak at 125 °C, which was attributed to loss of water molecules and decomposition of ammonium. The weight loss between 400 and 500 °C was 1.3% with no visible endothermic DTA peak. The second broad endothermic DTA peak appeared at 586 °C with the weight loss 12% between 500 and 600 °C, which was attributed to the dehydroxylation and the decomposition of surface sulfate groups. This is confirmed by XRF analysis in Table 1 that the content of sulfur had a big decrease on the catalyst of S/Ti-600.

For the sample of S/Zn-Ti (Fig. 9), the weight loss below 200 °C was 13.6% accompanied with the big endothermic DTA peak at 86 °C which due to the loss of physical absorbed water. The weight loss was about 3.9% between 200 and 400 °C, and was 2.1% between 400 and 600 °C, accompanied with the two minor peaks around 300 and 600 °C, which were due to the dehydration of water from micro pores, decomposition of acetate and ammonium and subsequently dehydroxylation of the sample. Incorporating of ZnO into TiO_2 increased the thermal stability of the impregnated surface sulfate species when compared to that of TiO_2 alone. It is also reported in the literature that the thermal stability of the sulfated materials would be influenced when zirconia is mixed with other metal oxides [31]. Thus, the thermogravimetry studies revealed that the mixed metal oxides Zn and Ti enhanced the thermal stability of the S/Zn-Ti catalyst.

All catalysts were analyzed by XRF spectrometry for quantitative determination of sulfur content, which is listed in Table 1. A comparison between the sulfur content in catalysts calcined at different temperatures shows that the sulfur content of S/Zn has been

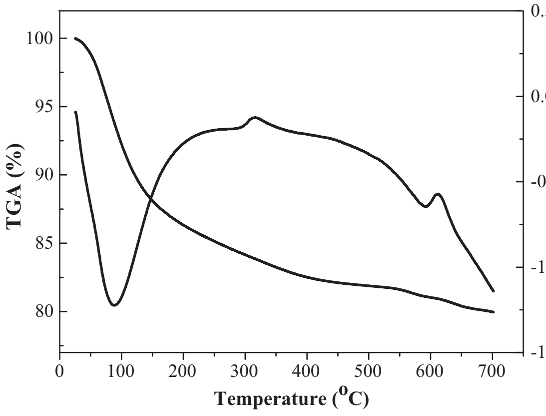

Fig. 9. TG/DTA curves of S/Zn-Ti.

Table 2
Textural and acid properties of S/Zn catalysts calcined at different temperatures.

S/Zn-°C	S_{BET} (m^2/g)	Pore volume (cm^3/g)	Mean pore diameter (nm)	Total acid amount (mmol g^{-1})
200	6.1	0.032	9.9	3.48
300	6.7	0.046	13.6	0.81
400	6.9	0.030	8.7	0.26
500	6.7	0.026	7.9	0.23
600	6.4	0.025	7.7	0.14

Table 3
Textural and acid properties of S/Ti catalysts calcined at different temperatures.

S/Ti-°C	S_{BET} (m^2/g)	Pore volume (cm^3/g)	Mean pore diameter (nm)	Total acid amount (mmol g^{-1})
200	13.9	0.013	3.6	3.91
300	22.2	0.016	2.9	2.16
400	33.0	0.023	2.7	1.72
500	68.0	0.059	3.5	0.54
600	55.6	0.120	8.6	0.13

decreased gradually during increasing the calcination temperature. For the samples of S/Ti, the sulfur content has a sharp decrease on S/Ti-600. However, the sulfur content in the mix oxides of Zn-Ti has been maintained stable.

3.1.4. *BET specific surface area analysis*

The BET specific surface area, pore volume and mean pore diameter of the catalysts S/Zn, S/Ti and S/Zn-Ti are summarized in Tables 2, 3 and 4, respectively. Primarily, catalysts with mesopore were preferred. For samples of S/Zn (Table 2), the specific surface area was relatively low (6.1–7.0 m^2/g) and changed slightly with increasing the calcination temperature. This can be explained by XRD and Thermal results that the structure of compounds was stable and had little changes with increasing the calcination temperature. For the samples of S/Ti catalysts (Table 3), the specific surface area firstly increased and had a peak at 500 °C, then decreased when the calcination temperature was higher than 500 °C. Take the thermal analysis of S/Ti into consideration that there was decomposition of sample between 400 and 600 °C. This indicates that more pores were produced when the catalyst calcined higher than 400 °C. As a result the specific surface area of S/Ti increased and had a peak at 500 °C. The slightly decreased surface area at higher calcination temperature may be primarily due to agglomeration of catalyst.

For the binary oxides S/Zn-Ti (Table 4), S/Zn-Ti-200 exhibited a high specific surface area 192 m^2/g. The high dispersion of binary oxides and/or the amorphous phase may contribute to the large specific surface area. The specific surface area decreased with increasing the calcination temperature and had a sharp decrease on the samples of S/Zn-Ti-400–500. From XRD analysis this may be due to the increase of the amount of cubic $TiZn_2O_4$. And the aggregation of particles may also decrease the specific surface area.

Table 4
Textural and acid properties of S/Zn-Ti catalysts calcined at different temperatures.

S/Zn-Ti-°C	S_{BET} (m^2/g)	Pore volume (cm^3/g)	Mean pore diameter (nm)	Total acid amount (mmol g^{-1})
200	192.3	0.128	1.3	4.34
300	165.0	0.116	1.4	2.94
400	67.7	0.084	2.5	2.76
500	15.3	0.057	7.4	1.8
600	9.4	0.064	1.4	1.5

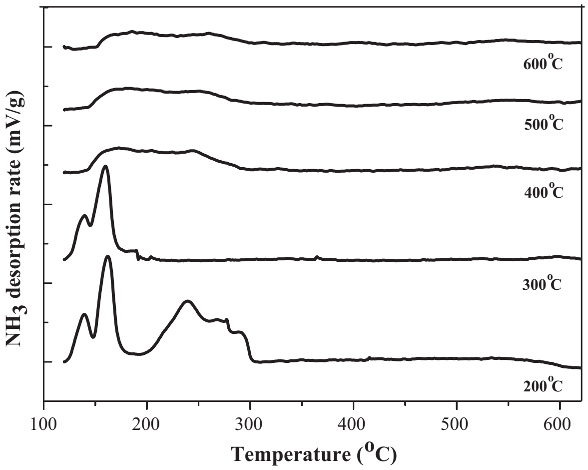

Fig. 10. NH_3–TPD curves for S/Zn calcined at different temperatures.

3.1.5. *Acid analysis*

The strength of acid and the total amount of acid sites on the surface of catalysts were determined by temperature-programmed desorption of adsorbed ammonia. From the thermogravimetry studies, there was the decomposition of sulfate or acetate which was also detected by conductivity detector (TCD). In order to distinguish the desorbed NH_3, blank experiments for each catalyst have been performed without ammonia admission under the same experimental conditions. The final NH_3–TPD signals were on the bases of blank signals.

The NH_3–TPD profiles of the series of S/Zn, S/Ti and S/Zn-Ti catalysts are shown in Figs. 7, 8 and 9, respectively. The peaks shown in each of the profiles correspond to desorption of NH_3 bound to the acid sites of oxide surface. The desorption temperature indicates the acid strength of the catalyst. The higher temperature of desorption, the stronger the acid strength. The NH_3–TPD profiles (Figs. 10–12) showed that all the catalysts mainly had two broad desorption peaks. One was between 150 and 400 °C, which corresponded to the weak and middle strength acid sites. The other was between 400 and 600 °C, which corresponded to the strong acid sites. For the series of S/Zn (Fig. 10), the intensity of peaks between 150 and 300 °C decreased distinctly with increasing the calcination temperature. It indicates that the weak acid sites predominated over the S/Zn catalysts. For the samples of S/Ti (Fig. 11), the NH_3 desorption peaks revealed continuous NH_3 desorption peaks in the range of 150–400 °C and intensive peaks between 450 and 600 °C.

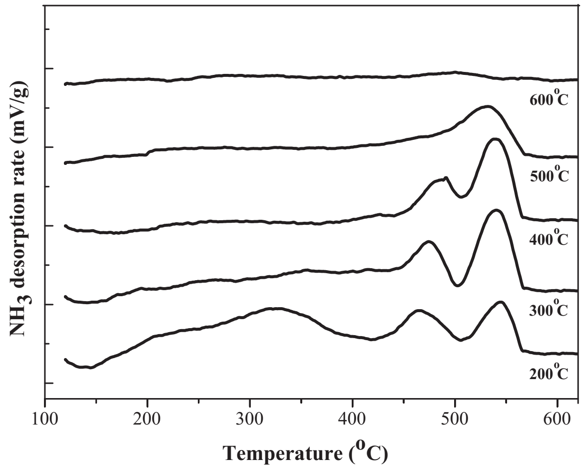

Fig. 11. NH_3–TPD curves for S/Ti calcined at different temperatures.

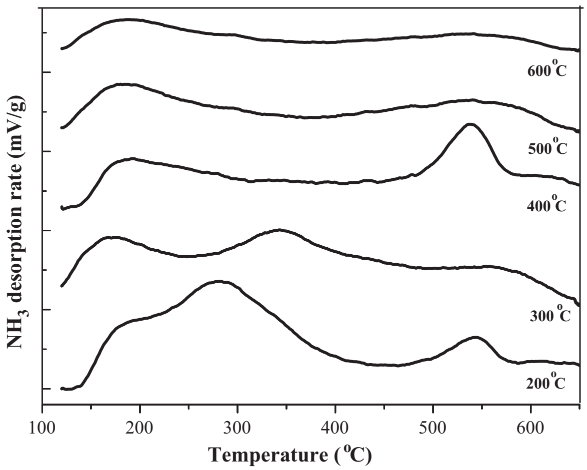

Fig. 12. NH$_3$–TPD curves for S/Zn-Ti calcined at different temperatures.

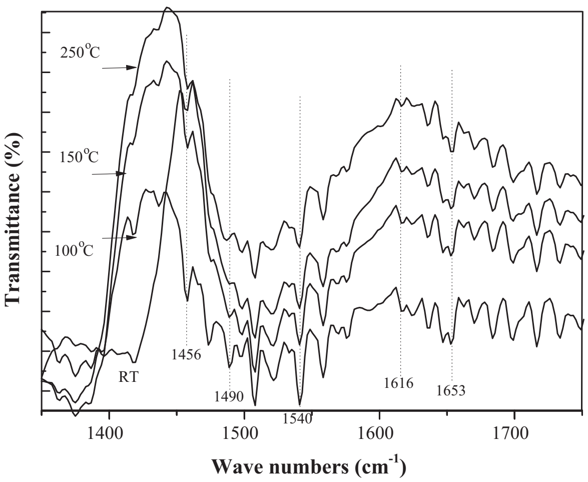

Fig. 14. FTIR spectra of pyridine adsorbed on S/Ti-300.

A large number of strong acid sites were presented on the samples of S/Ti-200–500. The NH$_3$ desorption peaks of the series of S/Zn-Ti (Fig. 12) were distributed between 150–400 °C and 400–600 °C with broad and over lapped desorption peaks. It indicates that the catalysts of S/Zn-Ti mainly signified a broad distribution of weak and middle strength acid sites on the surface of catalysts.

The acid amount corresponding to the amount of adsorbed NH$_3$ was estimated by integrating the area under the desorption peaks of NH$_3$–TPD. The total amount of acid for each series of S/Zn, S/Ti and S/Zn-Ti catalysts was listed in Tables 2, 3 and 4, respectively. The total amount of acid of these catalysts decreased with increasing the calcination temperature. The total amount of acid of S/Zn-Ti is more than that of S/Ti or S/Zn at each calcination temperature. It is supposed that the interaction between the different metal oxides could improve the generation of acid sites [32–34]. Therefore more surface acid sites could be expected on the binary oxides than Zn or Ti single metal oxide.

Infrared spectrum studies of pyridine adsorbed on solid surface have made it possible to distinguish between Brönsted and Lewis acid sites. Figs. 13, 14 and 15 show the FTIR spectra of the pyridine adsorbed at room temperature, 100 °C, 150 °C, and 250 °C on S/Zn-300, S/Ti-300 and S/Zn-Ti-300, respectively. Several bands were observed at around 1654 cm^{-1}, 1605 cm^{-1}, 1540 cm^{-1} and 1490 cm^{-1} as well as 1450 cm^{-1} in the region from 1700 cm^{-1} to 1300 cm^{-1}. The IR bands at 1654 cm^{-1} and 1540 cm^{-1} are assigned to the pyridine adsorbed on Brönsted acid sites and that at 1605 cm^{-1} is assigned to pyridine adsorbed with hydrogen bonding, the band at 1450 cm^{-1} is attributed to pyridine adsorbed on Lewis acid sites, and the IR band at 1490 cm^{-1} is attributed to both Brönsted and Lewis acid sites [35,36].

For the sample of S/Zn-300 (Fig. 13) the intensity of the band at 1453 cm^{-1} was distinctly strong, which ascribed to Lewis acid sites. However, with increasing the desorption temperature, the intensity of the band decreased a lot at desorption temperature 250 °C under vacuum. Generally, pyridine adsorbed on the weak acid sites desorbed at low temperature, and it adsorbed on strong acid sites desorbed at high temperature. This indicates that the Lewis acid was weak acid on the surface of S/Zn-300, which coincided with the result of NH$_3$–TPD. There were no distinct bands at 1654 and 1540 cm^{-1}, which indicated that there were few number of Brönsted acid sites on the surface of S/Zn-300. For the sample of S/Ti-300 (Fig. 14), the bands at 1654, 1540 and 1450 cm^{-1} were all observed. This indicates that there were both Brönsted and Lewis acid sites presented on the surface of S/Ti-300. For the sample of S/Zn-Ti-300 (Fig. 15), the band at 1450 cm^{-1} ascribed to Lewis acid sites was distinctly strong. However there were no obvious bands at 1654 and 1540 cm^{-1}. This indicates that there were few Brönsted acid sites and the Lewis acid sites predominated over S/Zn-Ti-300 catalyst. The intensity of acid features slightly decreased with increasing the desorption temperature. This indicates that the Lewis acid sites were strong on the S/Zn-Ti-300 catalysts. This is also confirmed by the NH$_3$–TPD results.

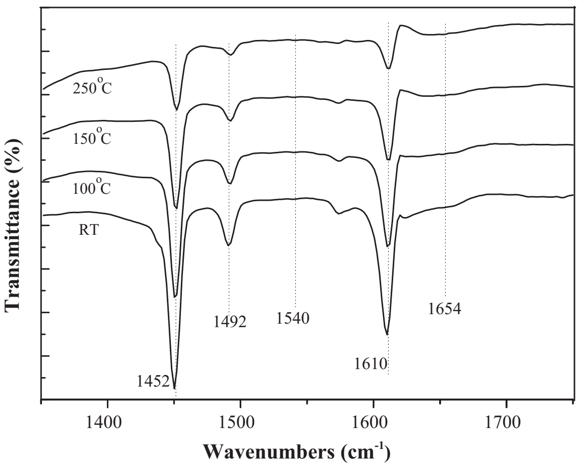

Fig. 13. FTIR spectra of pyridine adsorbed on S/Zn-300.

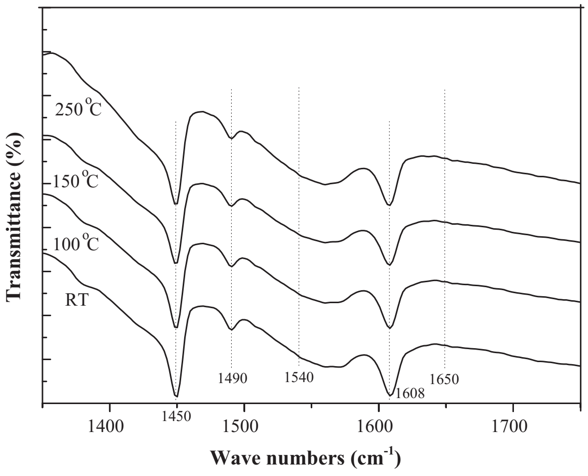

Fig. 15. FTIR spectra of pyridine adsorbed on S/Zn-Ti-300.

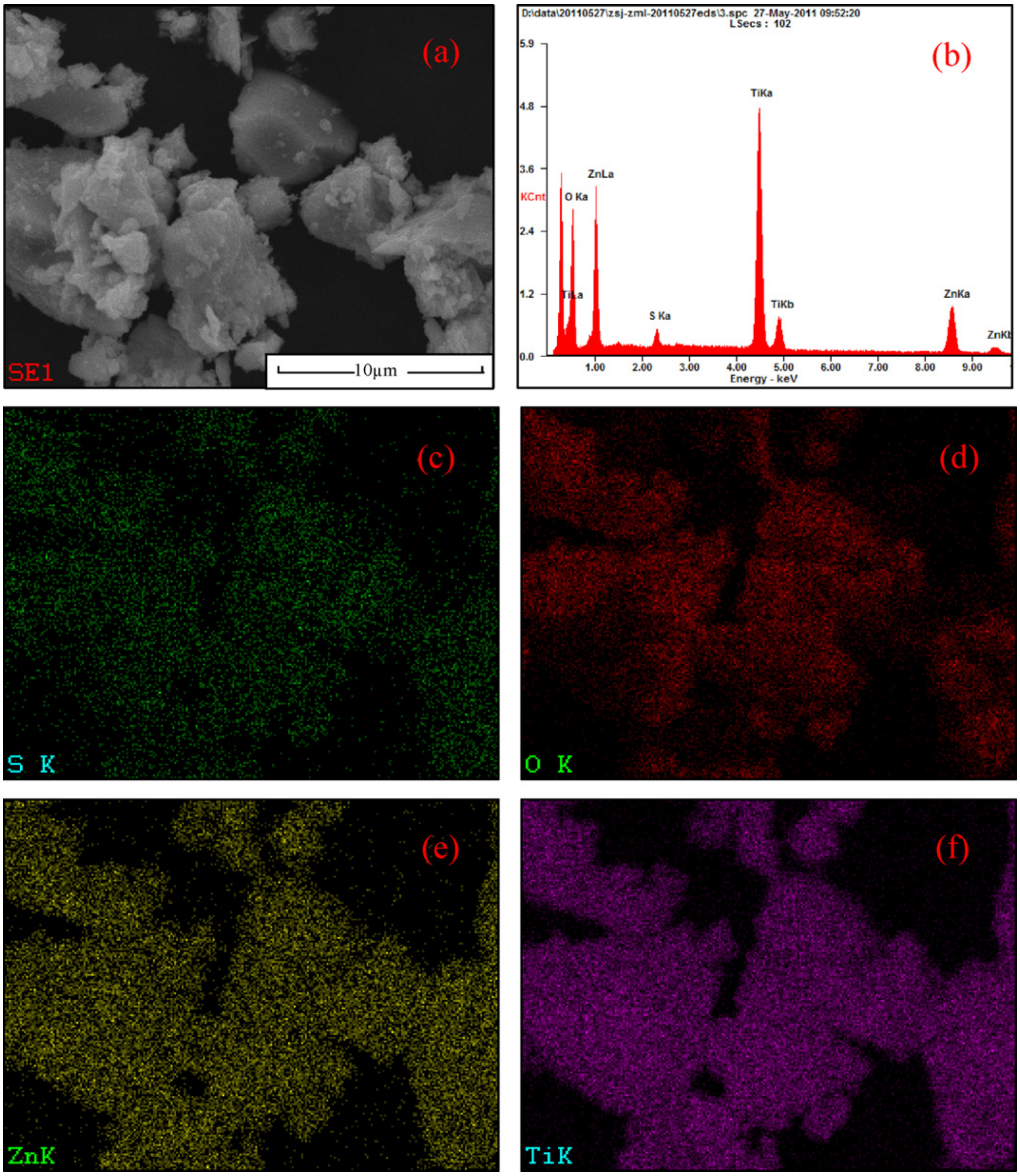

Fig. 16. The SEM and EDS of S/Zn-Ti-300: (a) SEM; (b) The element mass ratios; (c) EDS map of S; (d) EDS map of O; (e) EDS map of Zn; (f) EDS map of Ti.

3.1.6. SEM and EDS characterization

Fig. 16 showed SEM image and quantitative energy dispersive X-ray spectroscopy of the catalyst of SO_4^{2-}/Zn-Ti-300. It can be seen from Fig. 16(a) that the surface of SO_4^{2-}/Zn-Ti is smooth and some ultrafine crystallites have been also found. Quantitative analysis (Fig. 16(b)) shows the element mass ratios of Zn, Ti, O and S in the S/Zn-Ti-300 °C are 29.9%, 31.5%, 37.2 and 1.4%, respectively. Fig. 16(c–f) showed the density and distribution of the Zn, Ti, O and S elements on the catalyst evaluated by EDS mapping. As can be seen in Fig. 16, the elements of Zn, Ti, O and S are found to be homogeneously distributed on the whole surface. This indicates that the Zn and Ti species were highly dispersed in each other.

3.2. PET glycolysis reaction

3.2.1. Effect of calcination temperature

Calcination temperature is the key factor in synthesizing solid acid catalyst since it largely affects the structure and catalytic properties of catalyst. The effect of calcination temperature on catalytic activity of the series of S/Zn catalysts is shown in Fig. 17. The

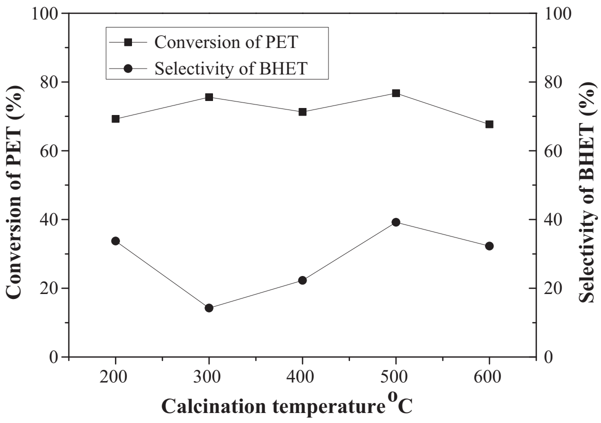

Fig. 17. Effect of calcination temperature of S/Zn on the conversion of PET and selectivity of BHET.

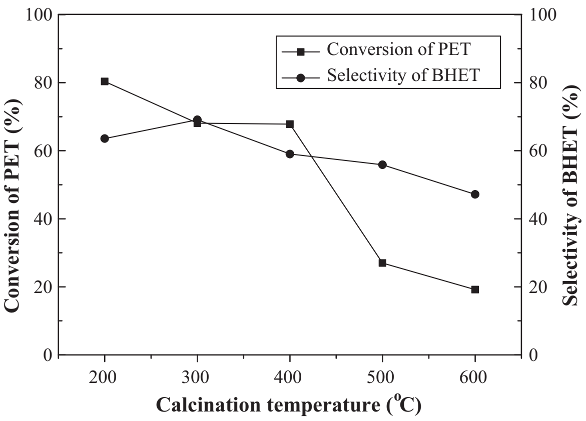

Fig. 18. Effect of calcination temperature of S/Ti on the conversion of PET and selectivity of BHET.

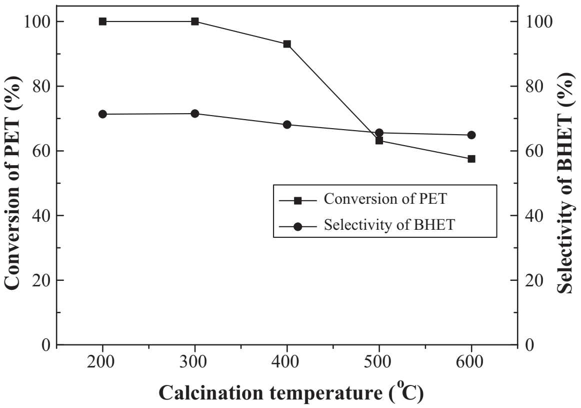

Fig. 19. Effect of calcination temperature of S/Zn-Ti on the conversion of PET and selectivity of BHET.

conversion of PET on the S/Zn catalysts at different calcination temperatures (200–600 °C) changed silghtly at around 70–80% but the selectivity of BHET were only at around 35%. There were no distinct changes between different calcination temperauture samples. From the textural analysis, the phase composition, crystalline structure and the specific surface area were changed slightly on the samples S/Zn-200–600. From the acid analysis, the amount of acid sites decreased distinctly with increasing the calcination temperature, and the acid strength was weak. The weak acid could not help to improve the catalytic activity. It also indicates that hexagonal ZnO might have weak interaction with sulfate ion, therefore few Lewis acid sites produced. Small surface area and few acid sites with weak strength might be the factors to inhibite its catalytic activity on the conversion of PET and the selectivity of BHET.

The catalytic activity of S/Ti catalysts is shown in Fig. 18. The results showed that the conversion of PET decreased from 80% to 20% with increasing the calcination temperature from 200 to 600 °C. There was a distinct decrease on the catalyst of S/Ti-500. From the textural analysis, the samples of S/Ti-200–400 mainly presented the amorphous and poor crystalline structure which showed higher activity than high crystalline of anatase TiO_2 presented on S/Ti-500–600. Further, the catalytic activity of S/Ti-200–600 followed the same sequence of the amount of surface acid sites on the catalysts. It showed that the acid amount made some contribution to the activity of catalyst. The largest specific surface area appeared on the S/Ti-500, however, the amount of acid sites were decreased, in this case the surface area could not help to improve the catalytic activity. The selectivity of monomer BHET had a slightly increase on the S/Ti-300 and then decreased with increasing the calcination temperature. Compared with catalysts of S/Zn, the catalysts of S/Ti calcined at low temperature improved the selectivity of BHET.

The effect of calcination temperature on the catalytic activity of the series of S/Zn-Ti catalysts is shown in Fig. 19. The conversion of PET was 100% on the catalysts S/Zn-Ti-200–300. The conversion of PET decreased with increasing the calcination temperature. And it had an obvious decrease on the catalyst of S/Zn-Ti-500. From the textural analysis, the catalysts of S/Zn-Ti-200–400 presented mainly the amorphous phase, which showed higher activity than high crystalline of anatase TiO_2 and cubic $TiZn_2O_4$ on S/Zn-Ti-500–600 in glycolysis of PET. Further, the catalytic activity of S/Zn-Ti-200–600 followed the same sequence of the total amount of surface acid and the specific surface area on the catalysts. It showed that the total amount of surface acid sites and the specific surface area might enhance the activity of catalyst. The selectivity of monomer BHET on the series of S/Zn-Ti was in the range of 65–71%, which changed slightly with increasing the calcination temperature.

In these three series catalysts S/Zn, S/Ti and S/Zn-Ti, S/Zn-Ti obviously improved the catalytic activity on the conversion of PET and the selectivity of BHET. The conversion of PET over S/Zn-Ti-200–300 was found to be 30% higher than that over S/Zn-200–300. And the selectivity of BHET over S/Zn-Ti was about one time higher than that over S/Zn at a wide range of calcination temperatures. On the S/Zn-Ti-200–400 the conversion of PET increased about 20–30% more than on the S/Ti-200–400 and on the S/Zn-Ti-500–600 about 40–50% more than on the S/Ti-500–600. Further, the selectivity of BHET over S/Zn-Ti-500–600 increased about three times higher than that over S/Ti-500–600. Take the catalysts' structure into consideration, the catalysts S/Zn-Ti-200–400 presented amorphous phase and the high dispersion of Zn and Ti species. Compared with XRD analysis of S/Zn and S/Ti, the binary oxides Zn-Ti inhibited the formation of crystalline structure until the calcination temperature reached the 500 °C. Further, the S/Zn-Ti calcined at low temperature presented high specific surface area and large amount of middle strength acid sites, therefore more active sites exposed, which is the main reason to improve the catalytic activity. The S/Zn-Ti calcined at high temperature presented the $ZnTi_2O_4$ compound which was due to the solid–solid reaction between ZnO and TiO_2. Therefore, more acid sites are expected to be produced on binary oxides (S/Zn-Ti) than that on single sulfated metal oxide (S/Zn or S/Ti). In conclusion, the large surface area, the amount of acid sites and the middle strength acid are the main factors to influence the glycolysis of PET and selectivity of BHET.

3.2.2. *Catalyst stability and reusability*

The reusability of S/Zn-Ti-300 was investigated and the experiment was followed by the procedure of Section 2.3. In order to determine whether the catalyst lost activity or not, the reaction time of 100% conversion of PET was recorded. The catalyst was recycled for four times. After the reaction, the catalyst was separated by centrifugation and reused without any further purification. The results of the recycling study are given in Table 5. For the fresh and recycled catalysts, it took about 180 min to achieve 100% conversion. Therefore, the catalytic activity of the recycled catalysts kept the same as that of the fresh catalyst and the selectivity of BHET maintained around 70–80%, which showed high stability of the catalyst in the reaction environment. Due to the high activity, selectivity and good reusability as well as low cost, the S/Zn-Ti-300 catalyst can be considered to be a promising catalyst for the glycolysis of PET.

3.2.3. *Effect of particle size*

The particle size has a key influence on heat and mass transfer phenomena and the effect of particle size on the conversion of PET

Table 5
Effect of the reused time of S/Zn-Ti-300 °C on the glycolysis of PET.

Cycle	Time of 100% conversion (min)	PET conversion (%)	BHET selectivity (%)	Production distributing (wt%)	
				BHET	Oligomers
Fresh	185	100	72.8	91.3	8.7
1st	181	100	74.1	91.6	8.4
2nd	175	100	77.5	91.9	8.1
3rd	168	100	77.4	91.8	8.2
4th	175	100	77.6	91.9	8.1

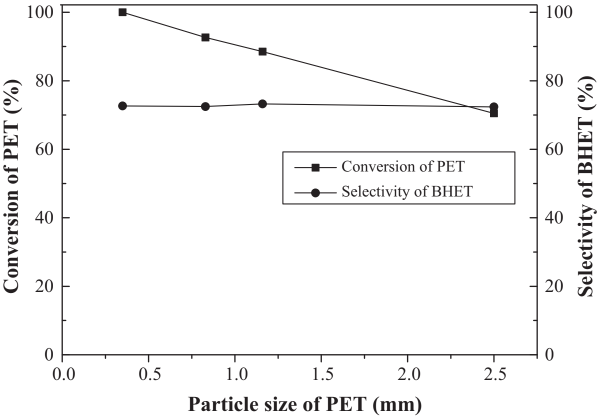

Fig. 20. Effect of particle size on the conversion of PET and selectivity of BHET.

and the selectivity of BHET is shown in Fig. 20. The reaction conditions were the same as that depicted in Section 2.3, except for reaction time, which was 2 h. The particle size of PET was varied from 0.35 to 2.5 mm. When the particle size was 0.35 mm and the reaction time was 2 h for 100% conversion of PET. With the particle size increased to 2.5 mm, the conversion of PET decreased gradually to 70.5%. The selectivity of BHET was kept stable around 70% with varying the particle size of PET.

4. Conclusion

Three series of catalysts S/Zn, S/Ti and S/Zn-Ti with different calcination temperatures had been tested for the glycolysis of PET. The characterization results suggest that the calcination temperature was a key factor to influence the textural properties, surface acidity and catalytic activity of the catalysts. Binary oxides of Zn and Ti inhibited the formation of crystalline in S/Zn-Ti until the catalysts calcined at 500 °C. The sulfated binary metal oxides (S/Zn-Ti) could develop more middle strength acid sites than single metal oxides (S/Zn or S/Ti). The amorphous structure, the high surface area and a large amount of middle strength acid sites are responsible for the excellent catalytic performance. Catalysts of S/Zn-Ti have dramatically improved the catalytic activity on conversion of PET and the selectivity of BHET. Under the conditions of 180 °C, atmospheric pressure, reaction time of 3 h, the conversion of PET was 100% and the selectivity of BHET was 72% on the catalysts of S/Zn-Ti-200–300 °C. The catalysts of S/Zn-Ti-200–300 °C are simple to prepare, have high reusability and are environmentally friendly. Therefore, S/Zn-Ti-200–300 °C are promising catalysts for the glycolysis of PET to BHET.

Acknowledgments

This work has been supported by National Natural Science Foundation of China (no. 21076221; no. 20976174) and National Basic Research Program of China (973 Program) (no. 2009CB219901).

References

[1] F. Welle, Twenty years of PET bottle to bottle recycling—an overview, Resources, Conservation and Recycling 55 (2011) 865–875.
[2] H. Wang, Y. Liu, Z. Li, X. Zhang, S. Zhang, Y. Zhang, Glycolysis of poly(ethylene terephthalate) catalyzed by ionic liquids, European Polymer Journal 45 (2009) 1535–1544.
[3] A. Carné Sánchez, S.R. Collinson, The selective recycling of mixed plastic waste of polylactic acid and polyethylene terephthalate by control of process conditions, European Polymer Journal 47 (2011) 1970–1976.
[4] E.S. Barboza, D.R. Lopez, S.C. Amico, C.A. Ferreira, Determination of a recyclability index for the PET glycolysis, Resources, Conservation and Recycling 53 (2009) 122–128.
[5] M.R. Patel, J.V. Patel, V.K. Sinha, Polymeric precursors from PET waste and their application in polyurethane coatings, Polymer Degradation and Stability 90 (2005) 111–115.
[6] O. Sato, K. Arai, M. Shirai, Hydrolysis of poly(ethylene terephthalate) and poly(ethylene 2,6-naphthalene dicarboxylate) using water at high temperature: effect of proton on low ethylene glycol yield, Catalysis Today 111 (2006) 297–301.
[7] G.M. de Carvalho, E.C. Muniz, A.F. Rubira, Hydrolysis of post-consume poly(ethylene terephthalate) with sulfuric acid and product characterization by WAXD, ^{13}C NMR and DSC, Polymer Degradation and Stability 91 (2006) 1326–1332.
[8] G.P. Karayannidis, D.S. Achilias, I.D. Sideridou, D.N. Bikiaris, Alkyd resins derived from glycolized waste poly(ethylene terephthalate), European Polymer Journal 41 (2005) 201–210.
[9] A. Mittal, R.K. Soni, K. Dutt, S. Singh, Scanning electron microscopic study of hazardous waste flakes of polyethylene terephthalate (PET) by aminolysis and ammonolysis, Journal of Hazardous Materials 178 (2010) 390–396.
[10] S.R. Shukla, A.M. Harad, Aminolysis of polyethylene terephthalate waste, Polymer Degradation and Stability 91 (2006) 1850–1854.
[11] R. López-Fonseca, I. Duque-Ingunza, B. de Rivas, S. Arnaiz, J.I. Gutiérrez-Ortiz, Chemical recycling of post-consumer PET wastes by glycolysis in the presence of metal salts, Polymer Degradation and Stability 95 (2010) 1022–1028.
[12] M.Y. Abdelaal, T.R. Sobahi, M.S.I. Makki, Chemical transformation of pet waste through glycolysis, Construction and Building Materials 25 (2011) 3267–3271.
[13] M.E. Viana, A. Riul, G.M. Carvalho, A.F. Rubira, E.C. Muniz, Chemical recycling of PET by catalyzed glycolysis: kinetics of the heterogeneous reaction, Chemical Engineering Journal 173 (2011) 210–219.
[14] G. Xi, M. Lu, C. Sun, Study on depolymerization of waste polyethylene terephthalate into monomer of bis(2-hydroxyethyl terephthalate), Polymer Degradation and Stability 87 (2005) 117–120.
[15] T.A. Peters, N.E. Benes, A. Holmen, Jos T.F. Keurentjes, Comparison of commercial solid acid catalysts for the esterification of acetic acid with butanol, Applied Catalysis A: General 297 (2006) 182–188.
[16] J.I. Moreno, R. Jaimes, R. Gómez, M.E. Niño-Gómez, Evaluation of sulfated tin oxides in the esterification reaction of free fatty acids, Catalysis Today 172 (2011) 34–40.
[17] D.E. López, J.G. Goodwin Jr., D.A. Bruce, E. Lotero, Transesterification of triacetin with methanol on solid acid and base catalysts, Applied Catalysis A: General 295 (2005) 97–105.
[18] J. Ni, F.C. Meunier, Esterification of free fatty acids in sunflower oil over solid acid catalysts using batch and fixed bed-reactors, Applied Catalysis A: General 333 (2007) 122–130.
[19] R. Sakthivel, H.A. Prescott, J. Deutsch, H. Lieske, E. Kemnitz, Synthesis, characterization, and catalytic activity of $SO_4/Zr_{1-x}Sn_xO_2$, Applied Catalysis A: General 253 (2003) 237–247.
[20] G. Fan, M. Shen, Z. Zhang, F. Jia, Preparation, characterization and catalytic properties of $S_2O_8^{2-}/ZrO_2$-CeO_2 solid superacid catalyst, Journal of Rare Earths 27 (2009) 437–442.
[21] D.E. López, K. Suwannakarn, D.A. Bruce, J.G. Goodwin Jr., Esterification and transesterification on tungstated zirconia: effect of calcination temperature, Journal of Catalysis 247 (2007) 43–50.
[22] M.K. Lam, K.T. Lee, A.R. Mohamed, Sulfated tin oxide as solid superacid catalyst for transesterification of waste cooking oil: an optimization study, Applied Catalysis B: Environmental 93 (2009) 134–139.
[23] C. Zhang, T. Liu, H. Wang, F. Wang, X. Pan, Synthesis of acetyl salicylic acid over WO_3/ZrO_2 solid superacid catalyst, Chemical Engineering Journal 174 (2011) 236–241.

[24] H. Wang, R. Yan, Z. Li, X. Zhang, S. Zhang, Fe-containing magnetic ionic liquid as an effective catalyst for the glycolysis of poly(ethylene terephthalate), Catalysis Communications 11 (2010) 763–767.

[25] A.J. Reddy, M.K. Kokila, H. Nagabhushana, J.L. Rao, C. Shivakumara, B.M. Nagabhushana, R.P.S. Chakradhar, Combustion synthesis, characterization and Raman studies of ZnO nanopowders, Spectrochimica Acta Part A 81 (2011) 53–58.

[26] R. Al Asmar, J.P. Atanas, M. Ajaka, Y. Zaatar, G. Ferblantier, J.L. Sauvajol, J. Jabbour, S. Juillaget, A. Foucaran, Characterization, Raman investigations on high-quality ZnO thin films fabricated by reactive electron beam evaporation technique, Journal of Crystal Growth 279 (2005) 394–402.

[27] C. Li, Y. Lv, L. Guo, H. Xu, X. Ai, J. Zhang, Raman and excitonic photoluminescence characterizations of ZnO star-shaped nanocrystals, Journal of Luminescence 122-123 (2007) 415–417.

[28] C.A. Chen, K.Y. Chen, Y.S. Huang, D.S. Tsai, K.K. Tiong, F.Z. Chien, X-ray diffraction and Raman scattering study of thermal-induced phase transformation in vertically aligned TiO_2 nanocrystals grown on sapphire(100) via metal organic vapor deposition, Journal of Crystal Growth 310 (2008) 3663–3667.

[29] P. Falaras, A.H.-L. Goff, M.C. Bernard, A. Xagas, Characterization by resonance Raman spectroscopy of sol–gel TiO_2 films sensitized by the $Ru(PPh_3)_2(dcbipy)Cl_2$ complex for solar cells application, Solar Energy Materials & Solar Cells 64 (2000) 167–184.

[30] P. Li, C. He, J. Cheng, C.Y. Ma, B.J. Dou, Z.P. Hao, Catalytic oxidation of toluene over Pd/Co_3AlO catalysts derived from hydrotalcite-like compounds: effects of preparation methods, Applied Catalysis B: Environmental 101 (2011) 570–579.

[31] B.M. Reddy, P.M. Sreekanth, P. Lakshmanan, A. Khan, Synthesis, characterization and activity study of $SO_4{}^{2-}/Ce_xZr_{1-x}O_2$ solid superacid catalyst, Journal of Molecular Catalysis A: Chemical 244 (2006) 1–7.

[32] B.M. Reddy, P.M. Sreekanth, Y. Yamada, Q. Xu, T. Kobayashi, Surface characterization of sulfate, molybdate, and tungstate promoted TiO_2-ZrO_2 solid acid catalysts by XPS and other techniques, Applied Catalysis A: General 228 (2002) 269–278.

[33] B.M. Reddy, B. Chowdhury, P.G. Smirniotis, An XPS study of the dispersion of MoO_3 on TiO_2-ZrO_2, TiO_2-SiO_2, TiO_2-Al_2O_3, SiO_2-ZrO_2, and SiO_2-TiO_2-ZrO_2 mixed oxides, Applied Catalysis A: General 211 (2001) 19–30.

[34] M.E. Manríquez, T. López, R. Gómez, J. Navarrete, Preparation of TiO_2-ZrO_2 mixed oxides with controlled acid-basic properties, Journal of Molecular Catalysis A: Chemical 220 (2004) 229–237.

[35] Z.M. El-Bahy, R. Ohnishi, M. Ichikawa, Hydrolysis of CF_4 over alumina-based binary metal oxide catalysts, Applied Catalysis B: Environmental 40 (2003) 81–91.

[36] G. Wang, Q. Liu, W. Su, X. Li, Z. Jiang, X. Fang, C. Han, C. Li, Hydroisomerization activity and selectivity of *n*-dodecane over modified Pt/ZSM-22 catalysts, Applied Catalysis A: General 335 (2008) 20–27.